ACS APPLIED MATERIALS & INTERFACES

Research Article

www.acsami.org

Controlled Synthesis of Homogeneous Ag Nanosheet-Assembled Film for Effective SERS Substrate

Tao Gao, Yongqiang Wang,* Ke Wang, Xiaoli Zhang, Jingna Dui, Gaomin Li, Shiyun Lou, and Shaomin Zhou

Key Laboratory for Special Functional Materials of the Ministry of Education, Henan University, Kaifeng 475004, P. R. China

Supporting Information

ABSTRACT: Homogeneous Ag nanosheet-assembled film was successfully fabricated by using Cu plate through a simple modified solution method, where weak reductive Cu_2O layer and complexing agent citrate ions were both introduced into the reaction system to control the reaction process. Meanwhile, citrate ions were used as morphology-controlled reagent to lead Ag units to grow in the form of nanosheet. The growth process exhibited that Ag nanosheet-assembled film formed slowly with reaction proceeding. Additionally, the pack density of nanosheets in the final product was found to be adjusted by the concentrations of Ag^+ ions in precursor solution. Using Rhodamine 6G (R6G) as probing molecules, the surface-enhanced Raman scattering (SERS) experiments showed that the Ag film assembled by nanosheets with high pack density exhibited excellent detecting performance, which could be used as effective SERS substrate for ultrasensitive detecting. Besides, a novel quintuplet SERS substrate could be synthesized in one batch by our method, which showed good reproducibility and a linear dependence between analyte concentrations and intensities, revealing the advantage of this method for easily scale-up production.

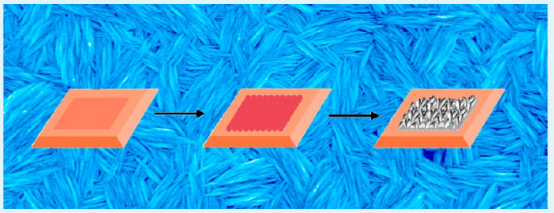

KEYWORDS: *surface-enhanced Raman Scattering, Ag nanosheet, film, solution method, detecting*

1. INTRODUCTION

Surface-enhanced Raman scattering (SERS), as a powerful and extremely sensitive analytical technique, has attracted wide attention since its first observation on a rough Ag electrode,[1] and has been intensely explored nowadays in the area of biodetection, biomedicine, environmental monitoring, analytical chemistry, etc.[2−5] Much research has demonstrated that the Raman signals could be enhanced greatly when target molecules reside in the gaps between neighboring metal nanoscaled units (so-called "hot spots"),[6−8] and the enormous enhancement endows the exquisite sensitivity of SERS, allowing the acquisition of the characteristic fingerprint of target molecules at low concentrations, even down to the single molecule level.[9]

For practical application of the SERS techniques, SERS substrates need to be reproducible, highly sensitive, facilely fabricated, and so on.[10] However, the Au and Ag electrodes or colloidal suspensions generally result in irreproducible SERS signals for the random distribution of "hot spots".[11,12] To date, various kinds of SERS substrates have been developed successively.[13−15] Among them, homogeneous SERS substrates with good signal reproducibility became the focus, which were realized through top-down nanopatterning techniques such as electron beam lithography and atomic layer deposition assisted with optical lithography.[16,17] However, these techniques were limited by their high cost and low throughput. Nowadays, tremendous efforts are continuously devoted to developing simple methods for homogeneous SERS substrates,[18−23] like electrochemical deposition and conductive polymer-assisted method, where the obtained uniform micro/nanostructured noble metal films not only had excellent sensitivity for high density of "hot spots", but also exhibited structural stability and reproducibility. For instance, Xu et al. reported the synthesis of homogeneous Ag film by using conducting polymer membrane as reducing agent;[18,19] Zhu and Liu et al produced Ag nanosheet-assembled films or microhemispheres via electrodeposition which showed good SERS performance like high sensitivity and reproducibility.[20−22] Although the above methods could be used to synthesize homogeneous SERS substrates, simpler and more low-cost approaches are still relentlessly pursued.

Simple solution methods like galvanic displacement are one of the best choices for their easy manipulations and potentially scale-up production. However, irregular product like Ag dendritic nanostructures were usually produced by direct using Cu, Al, and other plates as substrate,[24−26] which was mainly ascribed to their high reactivity (for example, Ag^+/Ag pair, 0.80 V, and Cu^{2+}/Cu pair, 0.34 V vs standard hydrogen electrode (SHE)[27]). Zhan et al. reported the synthesis of Ag nanoplates on Cu plate by modified galvanic displacement; although 2-nitrobenzoic acid was used as a complexing reagent to slow the reaction, it was still too fast to control the morphology of the final product.[28] Recently, our group reported that Ag nanosheet-assembled hollow microcubes

Received: May 3, 2013
Accepted: July 5, 2013
Published: July 5, 2013

with controllable morphology could be realized by using Cu_2O microcubes as weak reducer and trisodium citrate as complexing agent.[29] Enlightened by the idea, homogeneous SERS substrates could be controllably synthesized by using the Cu plate based on two modifications. On the one hand, a Cu_2O layer was introduced onto the Cu plate as a weak reductive layer that could decrease the reaction rate (Cu^+/Cu pair, 0.52 V vs SHE), and on the other hand, trisodium citrate was chosen as complexing agent of Ag^+ ions to decrease the concentration of free Ag^+ ions in the precursor solution.

The detailed synthesis strategy was schematically illustrated in Scheme 1. The preparation process mainly involved two steps. In the first step, a, weak reductive Cu_2O layer was introduced onto Cu plate by immersing Cu plate into $CuSO_4$ solution, where Cu^{2+} ions could be reduced to Cu^+ ions by Cu plate through in situ redox reaction according to eq 1. Therefore, the Cu plate fully covered with Cu_2O layer could be easily obtained.

Scheme 1. Schematic Illustration about the Controlled Synthesis of Ag Nanosheet-Assembled Film on Cu Plate

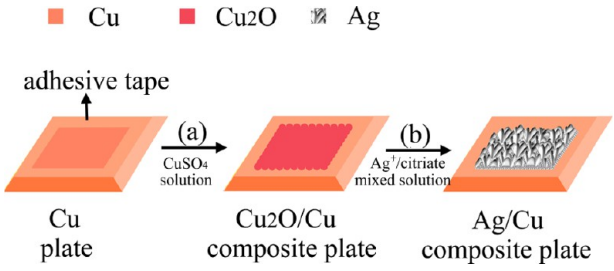

$$Cu^{2+} + Cu + H_2O \rightarrow Cu_2O + 2H^+ \quad (1)$$

In the second step, b, the Cu plate with Cu_2O layer was immersed into the mixed solution containing Ag^+ and citrate ions. The in situ generated Cu_2O weak reductive layer and citrate ions worked synergistically to slow down the reaction of the system. As we previously reported,[29] the concentration of H^+ (acidity of solution) could be used to adjust the reaction system according to eq 2, and then Ag film could be gradually formed through redox reaction under control.

$$2H^+ + Cu_2O + 2Ag^+ \rightarrow 2Ag + 2Cu^{2+} + H_2O \quad (2)$$

Additionally, citrate ions, a well-known morphology-directing reagent, also regulated the shape of the Ag units in the form of nanosheet. Through the above route, uniform Ag nanosheet-assembled film was expected to be fabricated by using Cu plate in a controlled way.

2. EXPERIMENTAL SECTION

2.1. Materials. Copper (Cu) plate, sodium dodecyl sulfate (SDS), silver nitrate ($AgNO_3$), trisodium citrate ($C_6H_5Na_3O_7{\cdot}2H_2O$), copper sulfate ($CuSO_4{\cdot}5H_2O$), and nitric acid ($HNO_3$) were purchased from Sinopharm Chemical Reagent Co., Ltd. All chemicals were of analytical grade and used without further purification. Water used throughout all these experiments was purified with a Millipore system.

2.2. Synthesis of Ag Nanosheet-Assembled Film on Cu Plate. *2.2.1. Introduction of Cu_2O Layer on the Cu Plate.* The Cu plate was first washed with acetone and ethanol to eliminate superficial contaminants in an ultrasonic bath, and rinsed with deionized water. After that, the surface was covered by adhesive tape, a window on the Cu plate was cut by knife, and the plate was then immersed into an aqueous solution of $CuSO_4$ (0.4 g, 50 mL) and SDS (0.1 g). After a while, the plate was taken out and rinsed with ethanol and deionized water repeatedly, and the Cu_2O/Cu composite plate was obtained for further use. The whole reaction was performed at room temperature and ambient pressure.

2.2.2. Synthesis of Ag Thin Film by Using Cu_2O/Cu Composite Plate. The Cu plate with Cu_2O layer was dipped into trisodium citrate solution (0.176 g, 70 mL) under magnetic stirring for a specific amount of time, then $AgNO_3$ solution (0.153 g, 5 mL) was added. After a while, dilute HNO_3 (10 mL, 2 mM) was injected into the above mixture quickly. 30 min later, the plate was rinsed with deionized water and ethanol several times, and saved in ethanol for further characterizations.

2.2. Characterizations. The morphology and composition of the as-prepared products were characterized by field-emission scanning electron microscopy (FESEM, JSM-7001F) at an acceleration voltage of 20.0 kV and energy dispersive X-ray spectroscopy (EDS). Transmission electron microscopy (TEM) observations were performed on a JEOL 2010 electron microscope operating at 200 kV. The phase and the crystallographic structure of the products were investigated by X-ray diffraction (XRD, Philips X0 Pert Pro).

2.3. SERS Measurements. Rhodamine 6G (R6G) dye were used as Raman probes for the SERS measurements. During the SERS tests, the Ag films were first immersed in 0.05 M KCl solution for 20 min to remove the possible impurities adsorbed on it, which might result in unwanted impurity peaks in the desired SERS spectra, and then a few

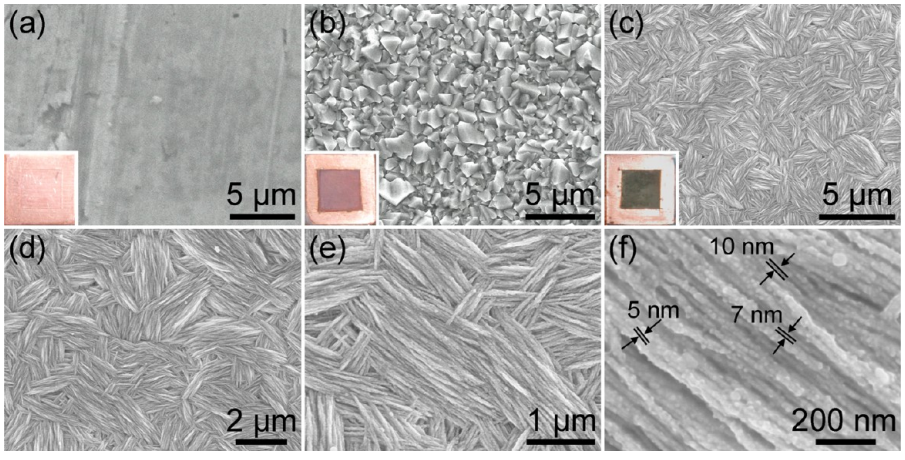

Figure 1. SEM images of: (a) Cu plate, (b) Cu_2O/Cu plate, and (c) Ag/Cu plate (the inset is the photo of the corresponding products); (d–f) the Ag nanosheets film with different magnifications.

of R6G solutions (200 μL) with different concentrations were used.[30] After 30 min, the substrates were rinsed with deionized water and ethanol carefully, and dried with high-purity flowing nitrogen. The substrates were measured under a confocal microscopy Raman Spectrometer (LABRAM-HR), using a laser beam with an excitation wavelength of 514.5 nm in this study. The acquisition time was 2 s for each spectrum. For each sample, we took three SERS spectra in different positions in the center area of the substrate and then averaged them.

3. RESULTS AND DISCUSSION

3.1. Morphology and Structure. Figure 1 presents typical scanning electron microscopy (SEM) images and photos of the products at every step in the above-mentioned method. As shown in Figure 1a, the surface of Cu plate is smooth and shows brass color in the inset of Figure 1a. After the Cu plate was treated in $CuSO_4$ solution, its color changed into cardinal red as seen in the inset of Figure 1b. A large area of the Cu_2O layer consisted of microcrystal particles are observed clearly on the surface of Cu plate in Figure 1b, and the grain sizes of the particles ranged from 0.5 to 3 μm. After immersed into the Ag^+ and citrate ions mixed solution for 30 min, gray color of the plate is found as shown in the inset of Figure 1c which implied the generation of Ag film. The morphology of the Ag film could be seen in Figure 1c, and large amount of nanosheets stacked compact together. In the high magnified SEM image (Figure 1d, e), the generated Ag film exhibits that these nanosheets are well-ordered locally in parallel while they entangle with each other in different directions as a whole. From high magnified SEM image in Figure 1f, it can be seen that these Ag nanosheets with average thickness of about 20−30 nm arranged randomly, and plenty of nanogaps with sub-10 nm are found between the parallel-linked nanosheets on the surface of Ag film. Additionally, energy dispersive X-ray spectroscopy (EDS) measurement was used to watch the changes of compositions in the above products. As shown in Figure S1 in the Supporting Information, the original Cu plate was transformed into Cu_2O/Cu plate successfully, which is revealed by the elemental changes from Cu (Cu plate, curve a) to Cu, O elements (Cu_2O/Cu composite plate, curve b), thereafter both Cu and Ag elements are detected in final product (Ag/Cu substrate, curve c), proving the generation of Ag. The morphologies and elements of products revealed that the reaction proceeded on the Cu plate according to the above designed steps. The cross-section of the Ag/Cu plate was further observed as shown in Figure S2a in the Supporting Information, where clear gap is also noticed between Cu substrate and the generated Ag film after reaction which indicated that Cu_2O layer participated in the reaction and was consumed after reaction. The thickness of Ag film was estimated to be around 2 μm in Figure S2b in the Supporting Information. Meanwhile, the close observation from the section of film (marked by rectangle in the inset of Figure S2b in the Supporting Information) further reveals that the film composed of compact stacked nanosheets.

The phase structure of the products was characterized by X-ray diffraction (XRD). The Cu plate with cubic structure (JCPDS No. 03−1005) was adopted in our experiment according to the diffraction peaks in curve a in Figure 2. After Cu_2O layer was introduced, clear signals of Cu_2O besides Cu plate were found from the indexed peaks (110), (200), (111) and (220) in curve b (JCPDS. No. 78−2076). The final product shows face-centered cubic Ag with two new peaks indexed as (111) and (220) according to JCPDS (No. 04−0783). Meanwhile, almost no peaks from Cu_2O were detected

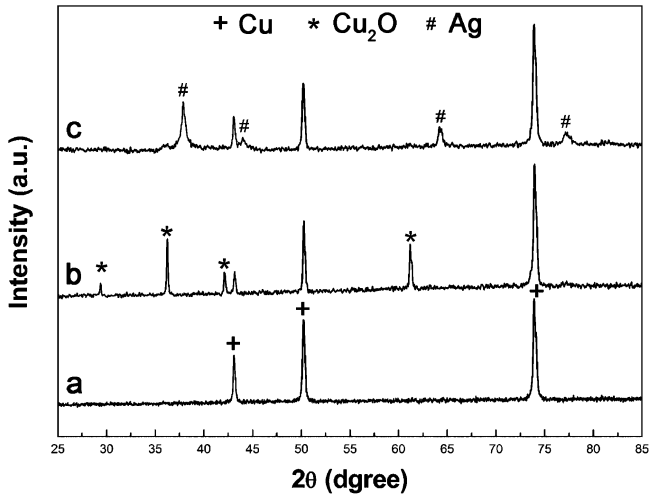

Figure 2. XRD patterns of (a) Cu plate, (b) Cu_2O/Cu composite plate, (c) Ag/Cu composite plate.

in curve c in Figure 2, which indicated the entire Cu_2O layer was consumed completely for the generation of Ag film during the reaction. The SEM images and XRD patterns proved that Ag nanosheet-assembled film had been successfully fabricated on Cu plate through chemical redox reaction.

3.2. Growth Process. Time-dependent experiments were conducted to watch the reaction process. Figure 3 shows the SEM images of the products obtained from 0 to 30 min. From images a and e in Figure 3, the Cu_2O film formed through in situ reaction exhibited multicrystalline structure with clearly crystal facets. After dilute HNO_3 solution (10 mL, 2 mM) was injected into the system, the reaction between Cu_2O and Ag^+ ions occurred slowly.[29] With the reaction time increasing to 3 min, a lot of Ag nanoparticles appeared on the surface of Cu_2O film in Figure 3b, f. As shown by the arrows tiny nanosheets could be observed which could be attributed to facet-inhibiting effect of citrate ions, since it was thought to preferentially adsorb on the {111} facets, inhibiting the growth of this plane.[31−33] Lots of previous experiments had also proved the morphology controlling effect of citrate ions during the growth of silver nanosheet.[34−36] These tiny nanosheets formed at the initial stage acted as nuclei center for the following growth, and the new generated bigger nanosheets aggregated into Ag film as shown in Figure 3c, which crossed each other and almost fully covered the Cu_2O layer. Meanwhile, it could be seen that the little tiny nanosheets grew along {111} facets with a length of about 700 nm after 8 min. Most of these nanosheets stacked together irregularly as shown in Figure 3g, whereas some local nanosheets stacked together face-to-face as the arrow marked in Figure 3g. When the reaction time was further prolonged to 30 min, the nanosheets grew along {111} facets continually and connected together into a complete and uniform Ag film in Figure 3d. Most of nanosheets were estimated to be about 1−3 μm in length, and these nanosheets weaved together with a "matting-like" surface. The Ag film was scraped from the substrate and broken under ultrasonication for TEM examination. As illustrated in Figure S3a in the Supporting Information, a broken sheetlike sample was observed, which was composed of large amount of small sheets as seen from the magnified edge of product shown in Figure S3b in the Supporting Information. TEM and selected area electron diffraction (SAED) provide further insight into the structure

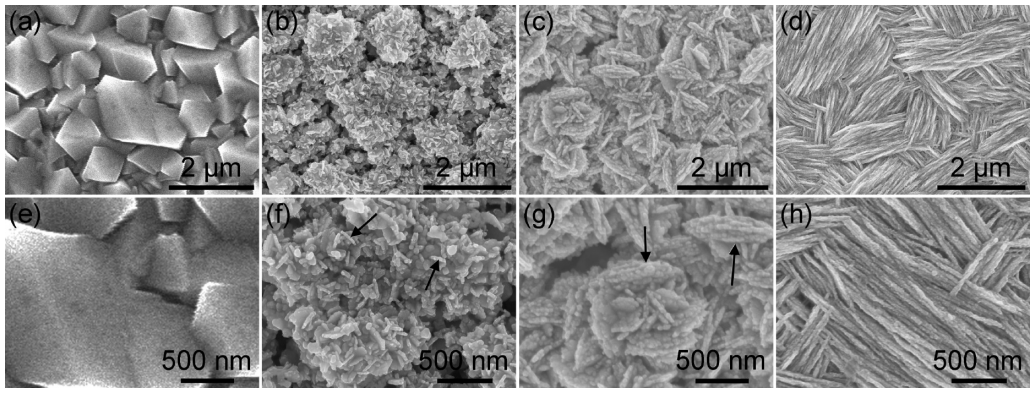

Figure 3. SEM images of the products obtained at different intervals: (a) 0, (b) 3, (c) 8, (d) 30 min; and (e–h) their corresponding magnified images.

of the Ag units. The lattice resolved TEM image (see Figure S3c in the Supporting Information) taken on a single Ag unit reveals fringes with a separated spacing of about 0.25 nm, being assigned to the 1/3{422} reflection which is generally forbidden for a face-centered cubic (FCC) lattice. Figure S3d in the Supporting Information is a typical SAED pattern where the hexagonal spot arrays can be assigned to the [111] orientation of the FCC structure, implying that the flat faces are bound by {111} planes. The spots marked with a square, circle and triangle in the SAED pattern can be indexed as {220}, 1/3{422} (formally forbidden Bragg reflections) and {422}, respectively. The SAED pattern also reveals that the planar surface of the nanosheet is parallel to {111}, because the electron beam was perpendicular to the surface of the sheet.[21] From the above reaction process, the Ag nanosheets grew slowly under the effect of citrate ions in the designed system, and the reaction proceeded in the similar way as reported previously.[29,37,38]

3.3. Influence of Ag^+ Concentrations on the Morphology. In our previous report, the amount of $AgNO_3$ played an important role in the tuning density of Ag nanosheets by using Cu_2O microcubes.[29] Here in this work, it was also found that the structure and morphology of the Ag products also strongly depended on the concentrations of $AgNO_3$ in the solution. We systematically investigated its influence on the morphology of the products through series of experiments while keeping the other conditions unchanged. Figure 4 showed the SEM images of the products obtained with different amount of $AgNO_3$. With the increasing in $AgNO_3$ from 0.051 to 0.153 g, two obvious changes including the density and size of nanosheets could be observed from Figure 4a–f. For example, the obtained product in images a and d in Figure 4 exhibited a sparse Ag nanosheet-assembled film with the length of single nanosheet around 500 nm, whereas the product in images c and f in Figure 4 showed a dense Ag nanosheet-assembled film with the length of single nanosheet around 2 μm. The reason could be proposed that the concentrations of $AgNO_3$ in the reaction solution strongly affected the density of Ag nuclei at the primarily stage and their subsequent growth, then sparse Ag nuclei on the plate inevitable lead to sparse distributed Ag nanosheet-assembled film. Besides, with the increasing concentrations of $AgNO_3$, the main structure of final Ag film gradually transitioned from cross-linked assembly to parallel-linked one.

3.4. SERS Measurement. Because of their unique shape, Ag nanosheets became the research focus for their displaying

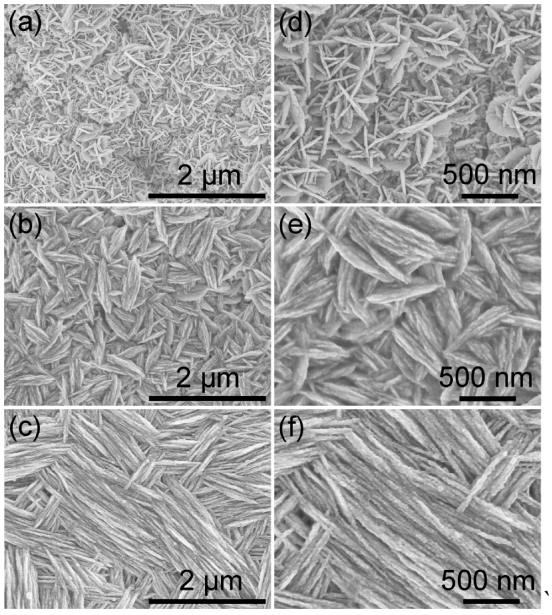

Figure 4. SEM images of the products obtained with different concentrations of $AgNO_3$: (a) 0.051, (b) 0.102, (c) 0.153 g; and (d–f) their corresponding magnified images.

LSPR over a broad range of wavelength and strong enhancement of the electromagnetic field at the sharp corners and edges of the nanosheets.[39−41] Especially, when the nanosheets assembled together, the nanogaps formed by paralleled or crossed nanosheets provided high density of "hot spots" which enhanced SERS signals greatly.[21,22] Therefore, the obtained Ag nanosheet-assembled film was expected to be utilized as desired substrates for SERS applications. The SERS performances of the above products were evaluated by using R6G as the model SERS marker; it needed to emphasize that only a little of analyte solution (200 μL) was used during the tests for trace detection. The Ag films with different pack densities of nanosheets in Figure 4 were first investigated as shown in Figure 5. Clear peaks were observed in the three curves, and the vibration peaks at 1187, 1311, 1363, 1509, and 1651 cm^{-1} could be assigned to C−H in-plane bending, C−O−C stretching, and C−C stretching of the aromatic ring of R6G molecule, respectively, while the peak at 773 cm^{-1} was due to the out-of-plane bending motion of the hydrogen atoms of the xanthene skeleton.[42] A clear enhanced effect at 1363 and 1651 cm^{-1} was observed in these spectra, which were the two main

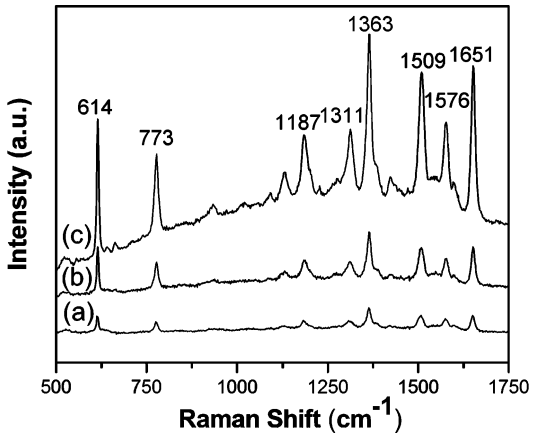

Figure 5. SERS spectra of R6G adsorbed on Ag films with different morphologies shown in (a) Figure 4a, (b) Figure 4b, (c) Figure 4c at 1 × 10^{-6} M.

characteristic peaks of R6G. Through comparing the signals and morphologies of the three products, we found that the film with highest pack density of Ag nanosheets demonstrated the SERS signals with highest intensity. As we know that the gaps between adjacent nanostructures in the sub-10 nm regime ("hot spots") is very critical to attain highly Raman-enhanced signals, which have been proved by both theoretical and experimental studies.[8,43] Here in our study, the sub-10 nm gaps existed in the intercrossed corners in the product shown in Figure 4a, and between the adjacent nanosheets in the product shown in Figure 4c. Obviously, the Ag film assembled by parallel-linked nanosheets provided more sub-10 nm gaps than that assembled by cross-linked nanosheets in the same area. Therefore, the plenty of "hot spots" located in the film in Figure 4c induced extremely enhanced Raman signals, which thus ensure the high sensitivity of the Ag nanosheet-assembled film as SERS substrates.

The SERS spectra of R6G at different concentrations were further measured by using the Ag film (Figure 4c) assembled by parallel-linked nanosheets as SERS substrate. As shown in Figure 6, the spectral intensities were decreased by diluting the concentrations of the target molecule. Many bands were distinctly observed from the inset of Figure 6 even when the

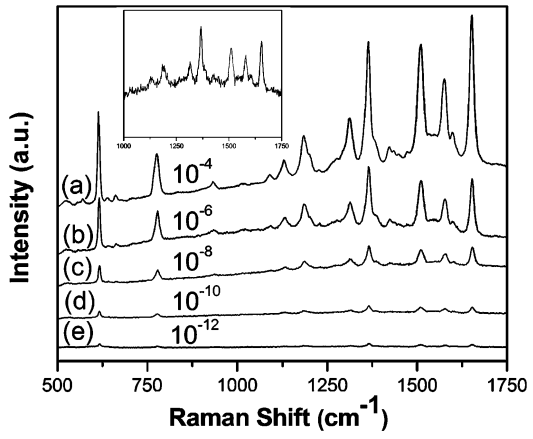

Figure 6. SERS spectra of R6G adsorbed on the product in Figure 4c with different concentrations: (a) 1 × 10^{-4} M, (b) 1 × 10^{-6} M, (c) 1 × 10^{-8} M, (d) 1 × 10^{-10} M, and (e) 1 × 10^{-12} M (the inset is a magnified curve of the SERS spectra at 1 × 10^{-12} M).

R6G concentration was reduced down to 1 × 10^{-12} M, demonstrating the high sensitivity of the Ag nanosheet-assembled film. These results confirmed that this kind of Ag nanosheet-assembled film could achieve ultra trace detection of analyte.

By taking R6G as the test molecule, the enhancement factor (EF) of the Ag film assembled by parallel-linked nanosheets as SERS substrate was estimated by the following eq 3[44]

$$EF = (I_{SERS}/I_{bulk})(N_{bulk}/N_{ads}) \quad (3)$$

where I_{SERS} and I_{bulk} are the Raman signals at a typical vibration (1363 cm^{-1} were chosen in our study) of the R6G molecules adsorbed on a substrate with the SERS effect and solid R6G molecules. N_{ads} and N_{bulk} are the numbers of the adsorbed molecules on Ag nanosheet-assembled film and the solid R6G molecules within the laser spot, respectively. In detail, for determination of N_{bulk} and N_{ads}, we spread the 20 μL R6G solution (10^{-3} M) onto a glass plate with 1 cm^2 and dropped the R6G solution (1 × 10^{-10} M, 200 μL) on the obtained Ag nanosheet-assembled film with area about 0.2 cm^2. Therefore, we can know the ratio N_{bulk}/N_{ads} was about 5 × 10^6 within the same area of laser spot. Then the above two samples were tested by Raman spectroscopy under same condition, and the results were shown in Figure S4 in the Supporting Information, and thus the ratio I_{SERS}/I_{bulk} could be calculated to be about 0.23 from the intensity of the corresponding peaks. Finally, the EF value was calculated to be about 1.15 × 10^6. The enhancement factor as high as 1 × 10^6 revealed the Ag nanosheet-assembled film could be used as effective SERS substrate in trace detection.

The reproducibility of the SERS signals using the obtained Ag/Cu plate as SERS substrate was validated as shown in Figure 7. The SERS spectra of R6G (1 × 10^{-8} M) were

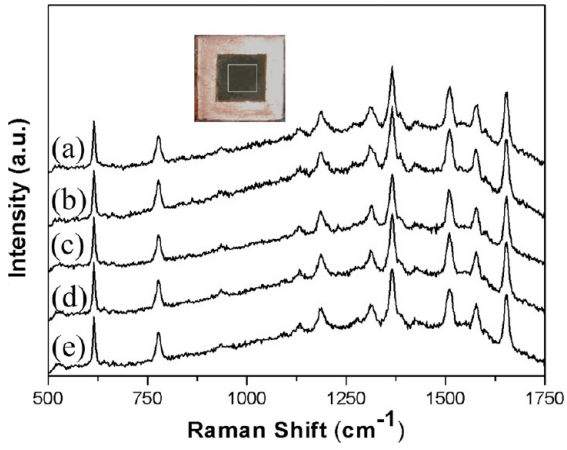

Figure 7. SERS spectra collected from five different spots in the center area of the Ag/Cu plate (inset image).

collected from center area as marked by rectangle in the inset of Figure 7. Seen from the five spectra in Figure 7, these SERS signals randomly collected from the center area in the Ag/Cu plate exhibited good similarity. Additionally, the relative standard deviation (RSD) was used to estimate the reproducibility of SERS signals. The RSD values of signal intensities of major SERS peaks were observed with the values below 0.2 in Table S1 in the Supporting Information, revealing a good reproducibility of Ag nanosheet-assembled film.[45] Interestingly, five windows in one Cu slide (quintuplet) could

be obtained easily by our method as shown inFigure S5 in the Supporting Information, and the SERS signals collected in center area of each windows also showed good similarity.

The quintuplet was also used as SERS substrate to investigate the relationship between intensities of SERS spectra and R6G concentrations. Five different concentrations were adopted and dropped onto these five windows in the experiment, and the relationship between the intensities and concentrations was drawn in Figure 8. A linear dependence was found between the

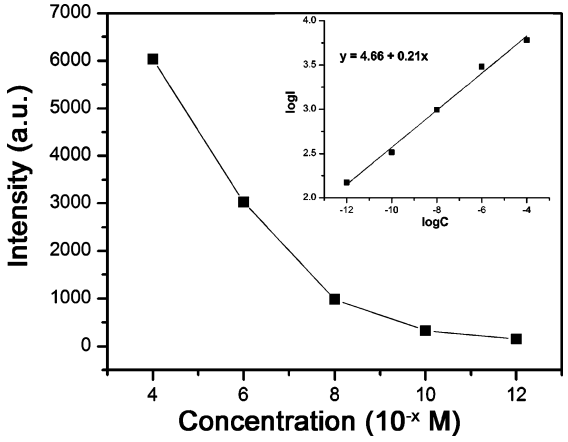

Figure 8. The relationship of peak intensities at 1363 cm^{-1} and concentrations of R6G. (The inset is the linear relationship between the logarithmic intensities and concentrations of R6G.).

logarithmic concentrations of R6G and the intensities of the fingerprint peak (1363 cm^{-1}) as shown in eq 4 below, where I is the peak intensity of the SERS spectra of R6G, and C is the concentration of R6G.

$$\log I = 4.66 + 0.21 \log C \quad (4)$$

4. CONCLUSION

In summary, we have presented a facile and new strategy for synthesis of Ag nanosheet-assembled film on Cu plate as SERS-active substrates, where the introduction of Cu_2O film as weak reductive layer and citrate ions as complexing agent made the growth process under control. The pack density of the Ag nanosheets on the Cu plate could be simply tuned by adjusting the concentration of $AgNO_3$. The SERS measurement results indicated the Ag film with high density of "hot spots" exhibited excellent performance. A novel quintuplet SERS substrate synthesized by our method demonstrated good reproducibility and a linear dependence between concentration and intensity. Therefore, our work has demonstrated a simple way to synthesize Ag nanosheet-assembled film as effective SERS substrate.

■ ASSOCIATED CONTENT

Supporting Information

EDS spectra of (a) Cu plate, (b) Cu_2O/Cu composite plate, and (c) Ag/Cu composite plate; normal Raman spectrum of pure R6G and SERS spectrum of R6G at the concentration of 1×10^{-10} M and Table of RSD values for the major peaks in SERS spectra of the R6G. This material is available free of charge via the Internet at http://pubs.acs.org.

■ AUTHOR INFORMATION

Corresponding Author

*E-mail: wangyq@henu.edu.cn.

Notes

The authors declare no competing financial interest.

■ ACKNOWLEDGMENTS

This work was supported by the Natural Science Foundation of China (51102077), the Doctoral Scientific Research Foundation of Henan University (B2010088), the Natural Science Foundation of Henan University (2010YBZR049).

■ REFERENCES

(1) Fleischmann, M.; Hendra, P. J.; McQuillan, A. J. *Chem. Phys. Lett.* **1974**, *26*, 163−166.
(2) Song, S.; Qin, Y.; He, Y.; Huang, Q.; Fan, C.; Chen, H. *Chem. Soc. Rev.* **2010**, *39*, 4234−4243.
(3) Kneipp, K.; Kneipp, H.; Itzkan, I.; Dasari, R. R.; Feld, M. S. *Chem. Rev.* **1999**, *99*, 2957.
(4) Camden, J. P.; Dieringer, J. A.; Zhao, J.; Van Duyne, R. P. *Acc. Chem. Res.* **2008**, *41*, 1653−1661.
(5) Graham, D.; Goodacre, R. *Chem. Soc. Rev.* **2008**, *37*, 883−884.
(6) McMahon, J. M.; Li, S.; Ausman, L. K.; Schatz, G. C. *J. Phys. Chem. C* **2012**, *116*, 1627−1637.
(7) Hao, E.; Schatz, G. C. *J. Chem. Phys.* **2004**, *120*, 357−366.
(8) Kovacs, G. J.; Loutfy, R. O.; Vincett, P. S.; Jennings, C.; Aroca, R. *Langmuir* **1986**, *2*, 689−694.
(9) Nie, S. M.; Emery, S. R. *Science* **1997**, *275*, 1102−1106.
(10) Lin, X. M.; Cui, Y.; Xu, Y. H.; Ren, B.; Tian, Z. Q. *Anal Bioanal Chem* **2009**, *394*, 1729−1745.
(11) Torres, E. L.; Winefordner, J. D. *Anal. Chem.* **1987**, *59*, 1626−1632.
(12) Suzuki, M.; Niidome, Y.; Kuwahara, Y.; Terasaki, N.; Inoue, K.; Yamada, S. *J. Phys. Chem. B* **2004**, *108*, 11660−11665.
(13) Fan, M.; Andrade, G. F.; Brolo, A. G. *Anal. Chim. Acta* **2011**, *693*, 7−25.
(14) Banholzer, M. J.; Millstone, J. E.; Qin, L.; Mirkin, C. A. *Chem. Soc. Rev.* **2008**, *37*, 885−897.
(15) Lal, S.; Grady, N. K.; Kundu, J.; Levin, C. S.; Lassiter, J. B.; Halas, N. J. *Chem. Soc. Rev.* **2008**, *37*, 898−911.
(16) Hatab, N. A.; Hsueh, C.; Gaddis, A. L.; Retterer, S. T.; Li, J.; Eres, G.; Zhang, Z.; Gu, B. *Nano Lett.* **2010**, *10*, 4952−4955.
(17) Im, H.; Bantz, K. C.; Lindquist, N. C.; Haynes, C. L.; Oh, S. *Nano Lett.* **2010**, *10*, 2231−2236.
(18) Yan, J.; Han, X.; He, J.; Kang, L.; Zhang, B.; Du, Y.; Zhao, H.; Dong, C.; Wang, H.; Xu, P. *ACS Appl. Mater. Interfaces* **2012**, *4*, 2752−2756.
(19) Xu, P.; Zhang, B.; Mack, N. H.; Doorn, S. K.; Han, X.; Wang, H. *J. Mater. Chem.* **2010**, *20*, 7222−7226.
(20) Zhu, C.; Meng, G.; Huang, Q.; Zhang, Z.; Xu, Q.; Liu, G.; Huang, Z.; Chu, Z. *Chem. Commun.* **2011**, *47*, 2709−2711.
(21) Zhu, C.; Meng, G.; Huang, Q.; Li, Z.; Huang, Z.; Wang, M.; Yuan, J. *J. Mater. Chem.* **2012**, *22*, 2271−2278.
(22) Liu, G.; Cai, W.; Kong, L.; Duan, G.; Lu, F. *J. Mater. Chem.* **2010**, *20*, 767−772.
(23) Sun, Y.; Wiederrecht, G. P. *Small* **2007**, *3*, 1964−1975.
(24) Chen, X.; Cui, C. H.; Guo, Z.; Liu, J. H.; Huang, X. J.; Yu, S. H. *Small* **2011**, *7*, 858−863.
(25) Gutés, A.; Carraro, C.; Maboudian, R. *J. Am. Chem. Soc.* **2010**, *132*, 1476−1477.
(26) Song, W.; Cheng, Y.; Jia, H.; Xu, W.; Zhao, B. *J. Colloid Interface Sci.* **2006**, *298*, 765−768.
(27) Lu, X.; McKiernan, M.; Peng, Z.; Lee, E. P.; Yang, H.; Xia, Y. *Sci. Adv. Mater.* **2010**, *2*, 413−420.
(28) Lai, Y.; Pan, W.; Zhang, D.; Zhan, J. *Nanoscale* **2011**, *3*, 2134−2137.

(29) Wang, Y.; Gao, T.; Wang, K.; Wu, X.; Shi, X.; Liu, Y.; Lou, S.; Zhou, S. *Nanoscale* **2012**, *4*, 7121−7126.
(30) Bell, S. E.; Sirimuthu, N. M. *J. Phys. Chem. A* **2005**, *109*, 7405−7410.
(31) Zeng, J.; Tao, J.; Li, W.; Grant, J.; Wang, P.; Zhu, Y.; Xia, Y. *Chem. Asian. J.* **2011**, *6*, 376−379.
(32) Kilin, D. S.; Prezhdo, O. V.; Xia, Y. *Chem. Phys. Lett.* **2008**, *458*, 113−116.
(33) Zhang, Q.; Li, N.; Goebl, J.; Lu, Z.; Yin, Y. *J. Am. Chem. Soc.* **2011**, *133*, 18931−18939.
(34) Wang, Y.; Wang, K.; Zou, B.; Gao, T.; Zhang, X.; Du, Z.; Zhou, S. *J. Mater. Chem. C* **2013**, *1*, 2441−2447.
(35) Zhang, B.; Xu, P.; Xie, X.; Wei, H.; Li, Z.; Mack, N. H.; Han, X.; Xu, H.; Wang, H. *J. Mater. Chem.* **2011**, *21*, 2495−2501.
(36) He, L.; Huang, J.; Xu, T.; Chen, L.; Zhang, K.; Han, S.; He, Y.; Lee, S. T. *J. Mater. Chem.* **2012**, *22*, 1370−1374.
(37) Li, Z.; Meng, G.; Huang, Q.; Zhu, C.; Zhang, Z.; Li, X. *Chem.—Eur. J.* **2012**, *18*, 14948−14953.
(38) Zhu, C.; Meng, G.; Huang, Q.; Huang, Z. *J. Hazard. Mater.* **2012**, *211*, 389−395.
(39) Zou, X.; Dong, S. *J. Phys. Chem. B* **2006**, *110*, 21545−21550.
(40) Pastoriza-Santos, I.; Liz-Marzan, L. M. *J. Mater. Chem.* **2008**, *18*, 1724−1737.
(41) Kelly, K. L.; Coronado, E.; Zhao, L. L.; Schatz, G. C. *J. Phys. Chem. B* **2003**, *107*, 668−677.
(42) Hildebrandt, P.; Stockburger, M. *J. Phys. Chem.* **1984**, *88*, 5935−5944.
(43) Fromm, D. P.; Sundaramurthy, A.; Schuck, P. J.; Kino, G.; Moerner, W. E. *Nano Lett.* **2004**, *4*, 957−961.
(44) Orendorff, C. J.; Gole, A.; Sau, T. K.; Murphy, C. J. *Anal. Chem.* **2005**, *77*, 3261−3266.
(45) Zhang, B.; Wang, H.; Lu, L.; Ai, K.; Zhang, G.; Cheng, X. *Adv. Funct. Mater.* **2008**, *18*, 2348−2355.